Hydrodynamic Model for Short Contact Time Circulating Fluidized Bed

A. Tinaburri
OLTEK Research Consortium, Kinetics Technology International SPA, Rome, Italy

Short contact time circulating fluidized beds (CFBs) are high-performance reactors with great potential of application for fast endothermic reactions. Optimal kinetic conditions require high operating temperature and very short residence time (~ 0.15 s), as well as plug flow in the reaction zone, and fast and efficient solid separation before quenching effluents. Hydrodynamics of dilute CFB operated at high gas velocity was simulated in isothermal condition. The gas-flow field is described using turbulence closure models developed for the single phase and modified to account for particle presence. Numerical computation was compared with experimental results of Arena et al. (1993) and Tinaburri et al. (1996) for two different riser configurations. A parametric analysis was performed to investigate inlet geometry influence on flow pattern along the riser. Internal tube and circumferential gas inlet produced the most promising configuration to realize optimal flow condition.

Introduction

A new technology is being developed that tries to use circulating fluidized bed (CFB) as a reactor for ultrafast endothermic reactions. One of the most interesting applications is related to steam cracking technology (Berg et al., 1989; Koyama et al., 1992). The unit consists of two risers (reactor and combustor) operating at different conditions (gas velocity, pressure), which exchange a solid stream through downcomers and feeders. Optimal conditions for reaction selectivity require high operating temperatures and very short residence times (~ 0.15 s), coupled with plug flow of gas and particles in the reaction zone. To fulfill these constraints, high gas velocities (up to 30 m/s at riser exit) and solid flux (up to 350 kg/s·m^2) are required, exceeding usual design limits of the CFB unit (gas velocity up to 8 m/s and solid flux up to 40 kg/s·m^2) and fluid catalytic cracking (FCC) plant (gas velocity up to 15 m/s at riser exit, residence time > 4 s) (Werther, 1993).

Available experimental results confirm the critical nature of the inlet section in determining the flow pattern for a riser operated at high gas velocity (Dry et al., 1992; Brereton and Grace, 1993). By increasing both gas and solid fluxes, the core-annulus flow structure is confined at the riser bottom, disappearing rapidly when gas velocity exceeds 10 m/s (Donsì and Sesti Osseo, 1993). Hence the idea of introducing the hydrocarbon feed along the riser, thereby contacting an upcoming solid stream transported by a carrier gas to concentrate the mixing zone into a relatively small volume.

Selectivity is dramatically affected by contacting device geometry (Bassi et al., 1993). Thus an accurate understanding of the turbulent flow behavior of a gas–solid mixture after the lateral gas inlet is necessary for accurate process design. Conventional one-dimensional (1-D) models, developed mostly while neglecting entrance and exit effects, are not reliable in predicting particle radial distribution along the riser, which is essentially for evaluating the reaction yield properly and selecting optimal riser geometry. On the contrary, most of available 3-D two-phase flow models deal with fully developed flow (Pita and Sundaresan, 1993; Bolio et al., 1995), and more sophisticated approaches increase the complexity and computational effort and still cannot be recommended as standard.

On these bases, a simplified approach has been attempted to describe the development of two-phase flow in dilute vertical risers operated at high gas velocity. The proposed model, which retains the essential features that characterize these flows, is subject to following main restrictions:

1. The solid phase is dilute and small enough to follow the fluid motion closely (particle diameter < 100 μm).

2. Turbulence is described using a two-equation K-ϵ model, only for continuous (gas) phase. The effect of the solid phase

on turbulence has been accounted for by adding a sink term in the transport equation (Chen and Wood, 1985, 1986). Although quite restrictive, these assumptions are justified by the low to moderate suspension density typical of a riser operated at high velocity.

In contrast to dense gas-particle flows, which are controlled by interparticle collisions, diluted flows are controlled by the local aerodynamic forces between the phases. The effect of turbulent eddies is to disperse suspended particles that are small enough to follow the turbulent motion of the gas. If the particles are small and light, they interact by the motion of interstitial gas, since this gas acts as a "buffer" that prevents contacts between solid surfaces (Sinclair and Jackson, 1989). In addition, for the current problem, typical Stokes numbers are larger, and the turbulence is not expected to be a critical factor (Tu and Fletcher, 1995). Model prediction of solid-phase radial volumetric fraction in proximity to the riser bottom entrance, where interparticle collisions are certainly not negligible, is therefore expected to be of limited validity. However, the influence of the secondary gas-inlet geometry on mixing phenomena downstream of lateral injection is fundamental in establishing reactor riser performance (Grace, 1990).

The objective of this study is to investigate the interaction between the gas–solid suspension rising from the bottom region and the gas stream coming from the lateral injection device. Numerical simulation has been carried out with the PHOENICS program (Rosten and Spalding, 1987), which is capable of solving fundamental flow equations with an Eulerian approach, as well as perform particle tracking (routine GENTRA).

Mathematical Model

In the Eulerian approach the two phases are considered to act macroscopically as continua, and separate (but coupled) equations of motion are solved for each phase. Volume-averaged equations of motion for the steady, developing flow of a gas–particle mixture are as follows:

Continuity:

$$\nabla(\epsilon_i \rho_i \boldsymbol{v}_i) = 0 \qquad i = s,g \tag{1}$$

Momentum balance:

$$\nabla(\epsilon_g \rho_g \boldsymbol{v}_g \boldsymbol{v}_g - \epsilon_g(\mu_g + \mu_T)\nabla \boldsymbol{v}_g) = -\epsilon_g \boldsymbol{i} \nabla P + \epsilon_g \rho_g \boldsymbol{g} + \epsilon_g \beta_{sg}(\boldsymbol{v}_s - \boldsymbol{v}_g) \tag{2}$$

$$\nabla(\epsilon_s \rho_s \boldsymbol{v}_s \boldsymbol{v}_s) = -\epsilon_s \boldsymbol{i} \nabla P + \epsilon_s \rho_s \boldsymbol{g} + \epsilon_s \beta_{sg}(\boldsymbol{v}_g - \boldsymbol{v}_s), \tag{3}$$

where

P = gas-phase pressure
g = gravitational acceleration
μ_g = gas-phase viscosity
μ_T = gas-phase turbulent or "eddy" viscosity
ρ_g, ρ_s = density of gas and solid, respectively
ϵ_g, ϵ_s = local average volume fraction of gas and solid, respectively ($\epsilon_s + \epsilon_g = 1$)
$\boldsymbol{v}_g, \boldsymbol{v}_s$ = local average velocity of gas and particles, respectively
β_{sg} = interphase drag function

$$\beta_{sg} = 1/2\ \rho_s A_p C_D |\boldsymbol{v}_s - \boldsymbol{v}_g|, \tag{4}$$

where

A_p = particle projected area: $(\pi/4)\ d_p^2$
C_D = drag coefficient given by Clift et al. (1978)

$$C_D = \frac{24}{Re_g}\left(1 + 0.15\, Re_g^{0.687}\right) + \frac{0.42}{\left(1 + 4.25\ 10^4\, Re_g^{-1.16}\right)}, \tag{5}$$

with Re_g defined as:

$$Re_g = \epsilon_g \rho_g |\boldsymbol{v}_s - \boldsymbol{v}_g| \frac{d_p}{\mu_g}.$$

Closure of the Reynolds stress is obtained assuming that the stress is related to the mean rate of strain through the eddy viscosity, determined by the Kolmogorov–Prandtl equation:

$$\mu_T = \rho_g C_\mu \frac{K^2}{\epsilon}, \tag{6}$$

where

ϵ = dissipation rate of turbulent kinetic energy
K = turbulent kinetic energy per unit mass

The intensity of the turbulent fluctuations and its dissipation can be found from the following transport equations, derived from single-phase flow relations modified to account for the presence of a dilute solid phase:

$$\nabla\left(\epsilon_g \rho_g \boldsymbol{v}_g K - \left(\mu_g + \frac{\mu_T}{\sigma_K}\right) \text{grad}\, K\right) = \epsilon_g \rho_s (P_K - \epsilon) + S_{K,p} \tag{7}$$

$$\nabla\left(\epsilon_g \rho_g \boldsymbol{v}_g \epsilon - \left(\mu_g + \frac{\mu_T}{\sigma_\epsilon}\right) \text{grad}\, \epsilon\right) = \epsilon_g \rho_g \frac{\epsilon}{K}(C_{1\epsilon} P_k - C_{2\epsilon} \epsilon) + S_{\epsilon,p}, \tag{8}$$

where

$C_{1\epsilon}, C_{2\epsilon}, C_\mu, \sigma_K, \sigma_\epsilon$ = empirically assigned constants with values typical of single-phase flow (Table 1)
P_K = kinetic turbulent energy production term by shear forces
$S_{K,p}, S_{\epsilon,p}$ = sources of K and ϵ due to the interaction between the phases

Table 1. Model Constants in the Turbulence Model

$C_{1\epsilon}$	1.44
$C_{2\epsilon}$	1.92
C_μ	0.09
σ_K	1.0
σ_ϵ	1.314

$S_{K,p}$, $S_{\epsilon,p}$ have been modeled according to Chen and Wood (1985):

$$S_{K,p} = \frac{2\epsilon_s \epsilon_g \rho_s K \left[1 - \exp\left(-\frac{B_k \tau_p}{\tau_e}\right)\right]}{\tau_p} \quad (9)$$

$$S_{\epsilon,p} = -\frac{\epsilon_s \epsilon_g \rho_s \epsilon}{\tau_p}, \quad (10)$$

where

B_k = empirical constant assigned a value of 0.0825

τ_p, τ_e = time scale characterizing the particle response and large-scale turbulent motion, defined according to Adeniji-Fashola and Chen (1990) as

$$\tau_p = \frac{d_p^2 \rho_s}{18\mu_g\left(\frac{C_D Re_g}{24}\right)} \quad (11)$$

$$\tau_e = \frac{0.165K}{\epsilon}. \quad (12)$$

The dispersed phase has also been modeled using a Lagrangian approach (GENTRA routine): a large number of particle trajectories are calculated using a previously computed fluid-velocity field. The continuous-phase momentum equation is solved taking into account the interphase source (momentum transfer due to drag force) computed by GENTRA. This approach is based on the PSI-cell method (Crowe et al., 1977). Particle motion is described by the equation:

$$\frac{dx_p}{dt} = u_p \quad (13)$$

where

x_p = particle position

u_p = particle velocity

Particle velocity is determined by the solution of the momentum equation:

$$m_p \frac{du_p}{dt} = \beta_{sg}(u_c - u_p) + m_p\left(1 - \frac{\rho_c}{\rho_p}\right)g - V_p \nabla p i, \quad (14)$$

where

u_c = continuous (gas) -phase average velocity

m_p = particle mass

β_{sg} = drag function, Eq. 4

V_p = particle volume

∇p = continuous-phase pressure gradient

Numerical integration follow the sequence: (a) calculation of Lagrangian time step; (b) motion of the particle solving Eq. 13; (c) calculation of particle velocity in the new position by solving Eq. 14; and (d) calculation of interphase source.

As the particles traverse each cell of the domain, exchange of momentum occurs.

The source of momentum that appears in the continuous-phase equation is

$$S_{\text{mom}} = \frac{\pi}{6}\Sigma\eta\left(\rho_s^o d_p^{o3} u_p^o - \rho_s^n d_p^{n3} u_p^n\right), \quad (15)$$

where the superscripts o and n denote the value at the beginning/end of the Lagrangian time step; η is the number of particles for that parcel; and Σ is the summation over all the time steps required for the particle to traverse the cell, and for all particles.

Riser Geometry

Focus has been restricted to the upflow vertical riser with lateral gas injection. Gas is introduced in the riser via a dual inlet: the primary gas stream is uniformly fed at the bottom and secondary through a circumferential inlet (Figure 1, configuration I). It's possible to specify circumferential gas inlet height and the angle of inclination of the velocity vector of the secondary stream.

An alternative geometry has been investigated providing a secondary gas inlet through riser circumference and one internal tube (Figure 1, configuration II).

Boundary Condition

All the incoming streams must be specified in terms of gas and solid mass flow rate, solid volume fraction, and gas physical properties. Inlet values of K and ϵ were generated according to Rizk and Elghobashi (1989):

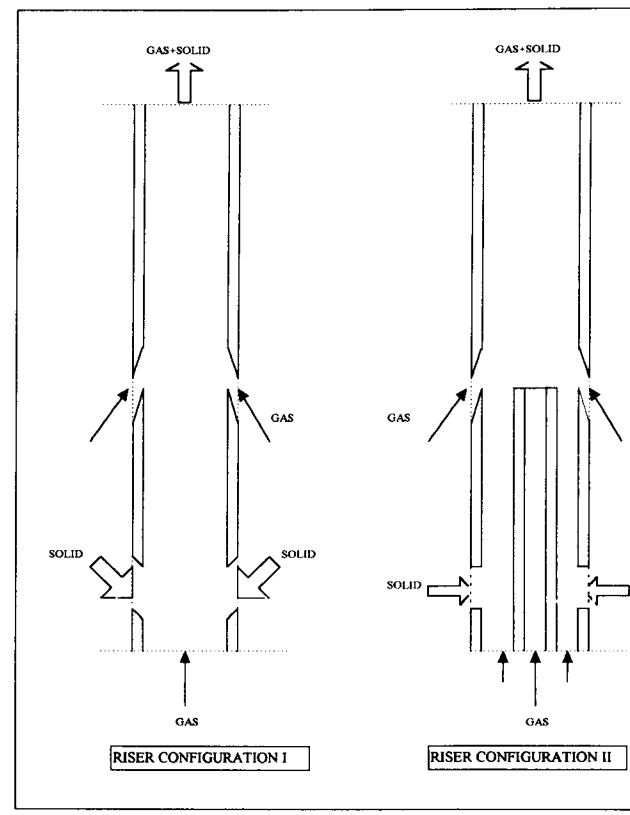

Figure 1. Riser geometry: circumferential gas inlet (I), circumferential and internal-nozzle gas inlet (II).

$$K_{in} = I^2 u_\infty^2 \tag{16}$$

$$\epsilon_{in} = \frac{C_\mu^{3/4} K_{in}^{3/2}}{l_m}, \tag{17}$$

where

I = turbulent intensity (typically in the range 0.01–0.05)
l_m = integral turbulence length scale equal to $0.1R$ (riser radius)
u_∞ = stream inlet velocity

At the axis of symmetry, all the radial gradients are set to zero. For small particles, Pita and Sundaresan (1991) and Dasgupta et al. (1994) pointed out that the wall boundary condition approximates closely the no-slip condition. We shall therefore demand that velocity vanish for both phases. In the Lagrangian scheme, particles trying to cross into a wall are bounced inside, modifying velocity as follows: the tangential component after bounce is the same as before, and the normal component is set to the negative of the same component before the bounce multiplied by the restitution coefficient e_w.

Because the closure model for Reynolds stresses is not valid in the viscous sublayer, boundary conditions at the wall have been obtained utilizing wall functions proposed for single-phase flow (considering the near wall layer in local equilibrium, as proposed by Patel et al. (1985)). This assumption (also adopted by Louge et al. (1991)) is justified by experimental evidence of the absence of solid recirculation at the wall. Some test simulations have revealed no particular advantage in adopting the low Reynolds number method (Lam and Bremhorst (1981)). Pressure is specified at the outlet section.

Computational Approach

The set of partial equations that express the conservation of mass and momentum in steady state is converted to finite difference and solved over a grid of control volumes that covers the domain of interest. The tubular reactor is defined by a 2-D polar grid. Discretized differential equations are solved iteratively (Rosten and Spalding, 1987). Convergence is controlled by observation of the field values of the dependent variables. As a further check on mass conservation, the inflows are compared with the net upflow at various heights along the riser. Computations were performed on a HP-Apollo series 7000 computer station.

Results and Discussion

Circumferential gas inlet (configuration I)

Let us first consider configuration I, reproducing the experimental apparatus utilized by Arena et al. (1991), henceforth referred to as the CNR case. The parameter values used in the model calculations are summarized in Table 2 (physical input data utilized in all subsequent simulations) and Table 3 (riser geometry and boundary conditions). The number of computational cells in the radial direction is equal to 20, in the axial direction to 58 (spaced more closely near gas inlets). It's worth noting that the momentum of the lateral gas stream relative to incoming gas–solid suspension can be higher or lower depending on the lateral inlet area.

Table 2. Physical Input Data

Particle type	Glass beads
Mean particle diameter	89 μm
Particle density	2,540 kg/m^3
Gas type	Air
Gas density	Compressible: MP/RT
Gas viscosity	$1.8E-5$ Pa·s
Temperature	20°C

Table 3. Geometrical Input Data and Boundary Conditions for Configuration I (CNR Case)

Riser radius	20.5 mm
Total riser height	6.4 m
Bottom inlet	
Solid mass flow	0.509 kg/s
Solid velocity (45° downward)	0.046 m/s
Gas axial velocity	5 m/s
Circumferential gas inlet	
Elevation along riser	3.14 m
Slot height	6 mm
Angle of inclination	30°
Gas velocity	17.0 m/s
Outlet section	
Outlet pressure	837 mm H_2O
Calculated axial gas velocity	15 m/s

Streams converging promote a redistribution of the kinetic and potential energies. An increase of the static pressure at the mixer inlet causes the lateral stream to form a toroidal vortex, whose dimension decreases reducing the stream's converging angle. This vortex confines the upcoming suspension near the riser axis. This effect may or may not interest the whole transversal section, depending on the lateral stream momentum, giving way to a sort of "volcano" or "Gaussian" shape in the contour plot of solid volumetric fraction (Figure 2). Kinetic energy is gained from potential in the converging part, and maximum velocities are reached a short distance downstream from the lateral injection device. According to this mechanism, mixing takes place after the expansion of the upflowing suspension. However, turbulent transport causes solid and gas flow to the wall (from dense core to dilute cylindrical annulus) (Arena et al., 1993).

Visual observation of the flow revealed the absence of solid recirculation at the riser-wall downstream lateral injection, due to high gas velocity. Pita and Sundaresan (1993) presented some results on a similar geometry. In their study, solid recirculation at the riser wall was observed due to lower gas velocity and a selected exit section boundary condition—gas and solid flowing radially—which is believed to promote solid recirculation (Clive et al., 1993). This feature is undesirable for thermal cracking of hydrocarbon feedstock and forces the reaction riser to operate at a higher gas velocity than required in a conventional unit. For this case, three different simulations were carried out: in the first, S_{kp} and $S_{\epsilon p}$ were set to zero (referred to as "zero source"); in the second, the Chen–Wood model was utilized; and in the third, the Lagrangian approach was adopted. Model predictions of experimental data of the riser pressure profile and laser-probe measurements of the radial particle volumetric fraction 0.6 m after lateral inlet are shown, respectively, in Figures 3 and 4. Axial pressure profile is nonlinear due to the vigorous exchange of momentum occurring soon after secondary inlet.

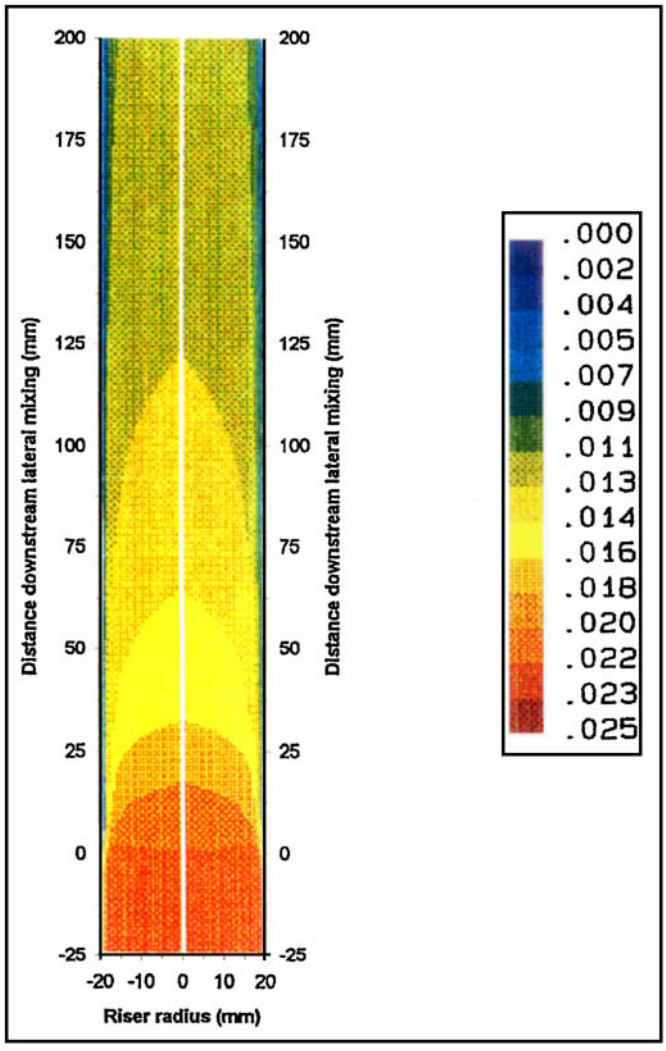

Figure 2. Contour plot of the model prediction of solid volume fraction after lateral inlet.

The conditions are specified in Tables 2 and 3. Configuration I (CNR case).

The interaction between two fluid streams impinging on each other produces energy dissipation and a sharp discontinuity in the pressure profile in the region around the injection point, mainly due to flow separation from the wall and the subsequent turbulent mixing. All proposed models agree well with pressure measurements.

Mixing between the two streams is almost completed 0.6 m after secondary injection, as shown in Figure 4, suggesting that the extinction of the mixing zone coincides with the onset of linear pressure decay downstream of the lateral inlet section. Model predictions of radial particle volumetric fraction obtained with GENTRA have been of lower quality due to the limited number of particles tracked (100 in order to achieve convergence with reasonable computational effort). Figure 5 shows that radial particle segregation is more pronounced for Zero source than for the Chen–Wood model, the former fitting better the experimental data. The Chen and Wood model failed to predict the correct trend because the present case is outside the range of applicability of this model. As with many aspects of turbulence modeling, parameters must be "tuned" to produce agreement with specific cases, and the parameters used for this simulation are believed not to be valid for this particular application. In this case, a look at the damping effect of the particles on the continuous-phase turbulence should be reduced, varying the value of the assigned empirical constant, B_k. Because of the good agreement obtained by neglecting the source terms in Eqs. 9 and 10, fine-tuning of the Chen–Wood model has not been carried out, and for all subsequent simulations only the Zero source model was used.

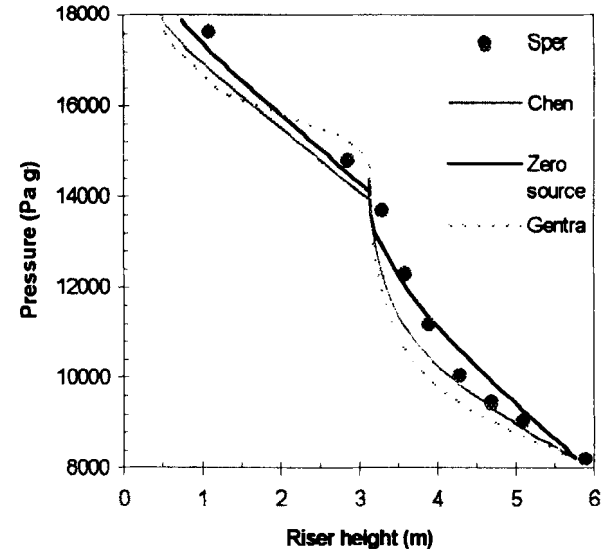

Figure 3. Model predictions of axial gas pressure vs. experimental data of Arena et al. (1991).

The conditions are specified in Tables 2 and 3. Configuration I (CNR case).

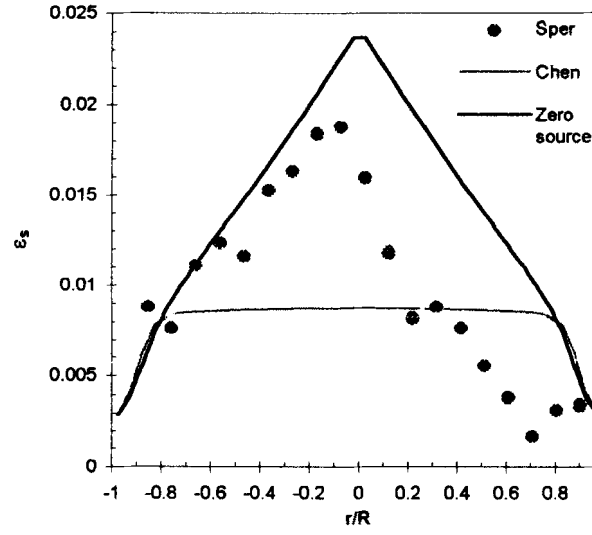

Figure 4. Model predictions of radial solid volume fraction 0.6 m after lateral inlet vs. experimental data of Arena et al. (1991).

The conditions are specified in Tables 2 and 3. Configuration I (CNR case).

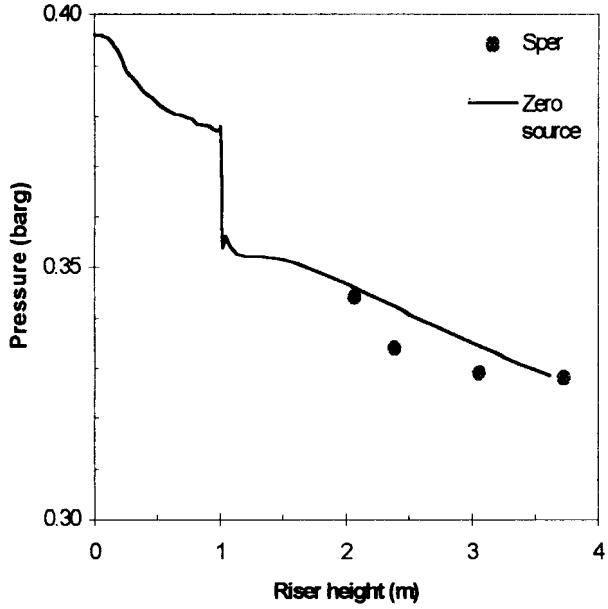

Figure 5. Model predictions of axial gas pressure vs. experimental data of Tinaburri et al. (1996).

The conditions are specified in Tables 2 and 4. Configuration I (OLTEK case).

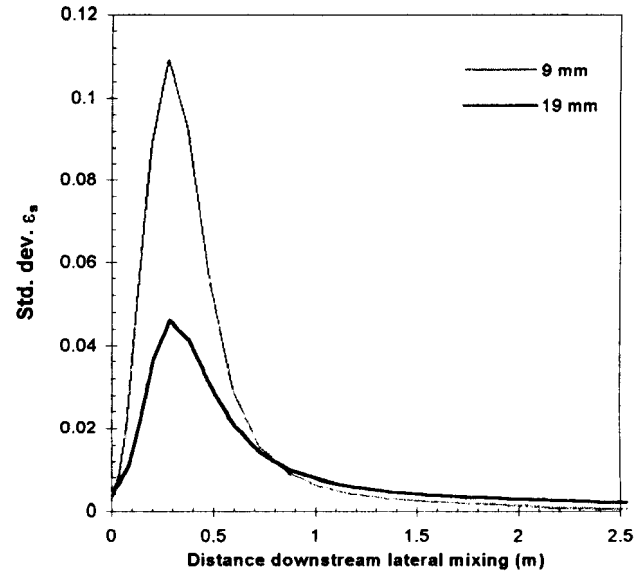

Figure 6. Model prediction of the effect of circumferential gas-inlet height.

The conditions are specified in Tables 2 and 4. Configuration I (OLTEK case).

Effect of lateral inlet geometry

Circumferential gas inlet direction and slot height are important variables in determining the flow pattern along the riser. A parametric study of the influence of these factors on solid radial segregation along the riser after the lateral inlet was carried out. The basic parameters for these simulations, reported in Table 4, have been selected in order to reproduce the operating conditions of an existing OLTEK cold pilot plant (gas velocity up to 35 m/s and solid flux up to 370 kg/s·m^2) (Tinaburri et al., 1996). The axial-pressure profile is available for the 19-mm circumferential slot height and 90° lateral inlet angle configuration, and model prediction of the experimental data is shown in Figure 5, again indicating good agreement.

In order to simplify comparison between the different configurations, numerical results have been synthesized using the standard deviation of the radial solid volumetric fraction in a certain section along the riser. This index was selected because of the Gaussian-like shape of the solid volumetric fraction downstream lateral mixing in order to allow simple evaluation of the degree of the fully developed flow condition and to give a qualitative indication of particle radial segregation along the riser. A zero value corresponds to the ideal case of uniform distribution.

Figures 6 and 7 show, respectively, the influence of the circumferential gas inlet height for a 90° inlet angle and of the lateral stream entering angle for a 9 mm slot height. In

Table 4. Geometrical Input Data and Boundary Conditions for Configuration I (OLTEK Case)

Riser radius	51 mm
Total riser height	4 m
Bottom inlet	
Solid mass flow	2 kg/s
Solid velocity (radial inward)	0.076 m/s
Gas axial velocity	6.9 m/s
Circumferential gas inlet	
Elevation along riser	1.0 m
Slot height	9–19 mm
Angle of inclination	60°–90°
Gas velocity	24.3–51.4 m/s
Outlet section	
Outlet pressure	0.318 barg
Calculated axial gas velocity	25.3 m/s

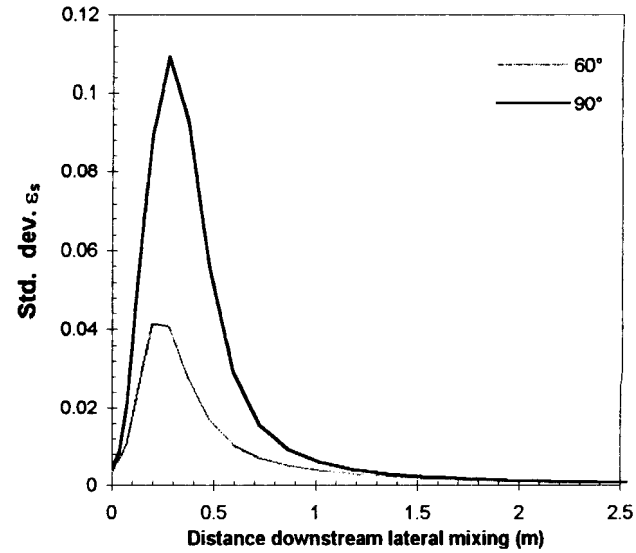

Figure 7. Model prediction of the effect of circumferential gas-injection direction.

The conditions are specified in Tables 2 and 4. Configuration I (OLTEK case).

all cases standard deviation increases soon after lateral inlet, reaches a peak, and then decreases uniformly along the riser height. Peak position and magnitude are sensitive to circumferential inlet geometry: reducing height or increasing angle causes the peak magnitude to increase and the peak axial position to shorten. This effect is easily explained, considering that both aforementioned actions increase the radial momentum component of the lateral stream. An asymptotic value is reached about 1.0–1.4 m downstream of the lateral mixing, indicating that a nearly fully developed flow condition has been achieved.

Based on a careful evaluation of the numerical computations and other experimental findings obtained at CNR (Arena et al., 1993), a simple criterion has been established in order to summarize research results by a "rule of thumb" for secondary inlet design. Mixing devices should be sized based upon the ratio of the lateral stream momentum radial component to the bottom upcoming suspension momentum: recommended values for optimal gas–solid mixing should be in the range 2–3. It's important to remark that scale up to reactor applications adds further complexity, as gas–solid mixing is coupled with the gas reagent's diffusion, because of the different compositions of the bottom and lateral streams.

Lateral and internal tube gas inlet (configuration II)

The parameter values concerning riser geometry and boundary conditions used in the model calculations are summarized in Table 5. The same gas and solid-mass flow rate adopted in previous simulations has been selected, splitting secondary gas into two equal streams, one to the internal tube and the other to the circumferential injection device.

Analysis of the contour plot of the volumetric particle fraction in Figure 8 clearly indicates the potential advantage of adopting this configuration in reducing the peak of ϵ_s in proximity to the riser axis. In this case, the tendency of the upcoming gas–solid stream to be confined close to the riser axis by interaction with the lateral stream is opposed by jet expansion upon leaving the internal nozzle. Suspension is initially confined in the annulus delimited between the internal tube and the riser radius, before starting to diffuse in the surrounding fluid. This explains the shape of the solid radial volumetric fraction downstream mixing presenting two peaks, as shown in Figure 9 for a section 0.5 m away from the lateral inlet. In order to facilitate comparison, model predictions obtained for configuration I using the same overall operating conditions have also been reported.

Configuration II allows a sensible reduction in the required mixing length to achieve an asymptotic value typical of the fully developed flow condition. Further experimental investigation on this geometry has been undertaken in order to confirm these findings.

Table 5. Geometrical Input Data and Boundary Conditions for Configuration II

Riser radius	51 mm
Riser height	4 m
Bottom inlet	
Solid mass flow	2 kg/s
Solid velocity (radial inward)	0.076 m/s
Gas axial velocity	10.5 m/s
Circumferential gas inlet	
Slot height	9 mm
Angle of inclination	60°
Gas velocity	25.5 m/s
Internal nozzle gas inlet	
Tube radius	30 mm
Gas axial velocity	26 m/s
Outlet section	
Outlet pressure	0.318 barg
Calculated axial gas velocity	25.3 m/s

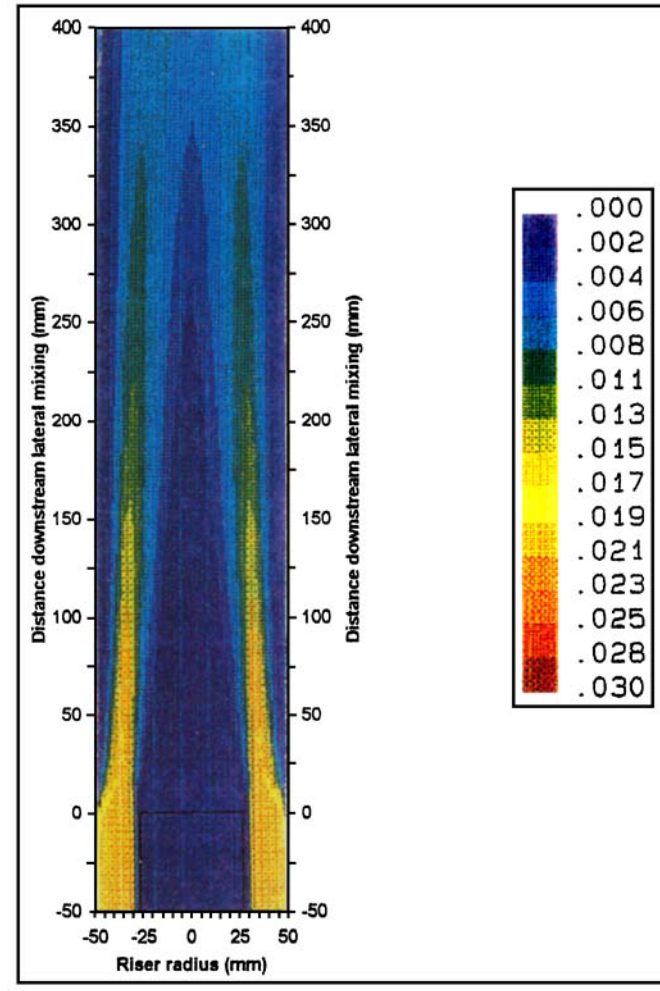

Figure 8. Contour plot of the model prediction of solid volume fraction after secondary inlet.

The conditions are specified in Tables 2 and 5. Configuration II.

Conclusions

The developing flow of a gas–solid mixture in a vertical cylindrical riser with secondary gas injection has been investigated. Two riser configurations were examined and numerical computations compared with available experimental results obtained at high gas velocity. A parametric study was performed to analyze the influence of inlet geometry on the flow pattern along the riser after the secondary inlet. For the selected operating conditions, no solid recirculation at the

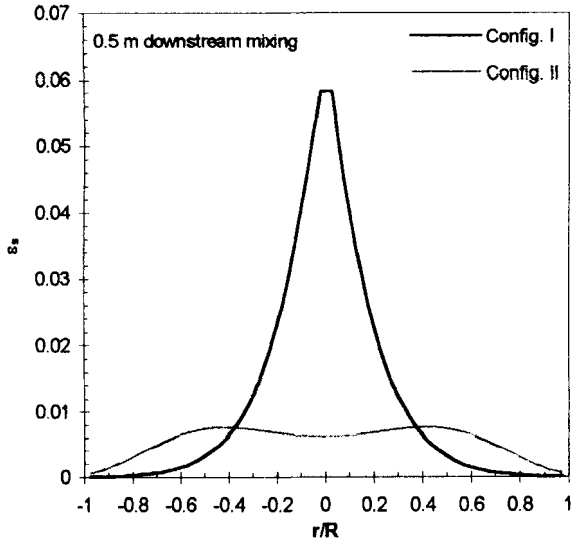

Figure 9. Model prediction of radial solid volume fraction 0.5 m after secondary inlet.

The conditions are specified in Tables 2 and 5. Configuration II.

riser wall has been observed after the streams mixed. The circumferential and internal tube gas inlet represented the most promising riser geometry in realizing optimal fluid dynamic conditions for short-contact-time endothermic reactors.

Acknowledgment

The author gratefully acknowledges funding support from the Ministero dell'Università e dell Ricerca Scientifica e Tecnologica as part of the PNRC project assigned to ENICHEM SpA. The author also thanks Professor Arena for kindly providing the experimental measurements, and M. Della Gora for his technical assistance.

Literature Cited

Adeniji-Fashola, A., and C. P. Chen, "Modelling of Confined Turbulent Fluid-Particle Flows Using Eulerian and Lagrangian Schemes," *Int. J. Heat Mass Transf.*, **33**, 691 (1990).

Arena, U., et al., Research Rep. for OLTEK, Rome (1991).

Arena, U., A. Marzocchella, and V. Bruzzi, "Mixing Between a Gas-Solid Suspension Flowing in a Riser and a Lateral Gas Stream," *Circ. Fluid. Bed Technol.*, **IV**, 545 (1993).

Bassi, A. S., C. L. Briens, and M. A. Bergougnou, "Short Contact Time Fluidized Reactors (SCTFRs)," *Circ. Fluid. Bed Technol.*, **IV**, 15 (1993).

Berg, D. A., C. L. Briens, and M. A. Bergognou, "Reactor Development for the Ultrapirolysis Process," *Can. J. Chem. Eng.*, **67**, 96 (1989).

Bolio, E. J., J. A. Yasuna, and J. L Sinclair, "Dilute Turbulent Gas-Solid Flow in Risers with Particle-Particle Interactions," *AIChE J.*, **41**, 1375 (1995).

Brereton, C. M. H., and J. R. Grace, "End Effects in CFB Hydrodynamics," *Circ. Fluid. Bed Technol.*, **IV**, 137 (1993).

Chen, C. P., and P. E. Wood, "A Turbulence Closure Model for Dilute Gas-Particle Flows," *Can. J. Chem. Eng.*, **63**, 349 (1985).

Chen, C. P., and P. E. Wood, "Turbulence Closure Model of the Dilute Gas-Particle Axisymmetric Jet," *AIChE J.*, **32**, 163 (1986).

Clift, R., J. R. Grace, and M. E. Weber, *Bubble, Drops and Particles*, Academic Press, New York, p. 111 (1978).

Crowe, C. T., M. P. Sharma, and D. E. Stock, "The Particle-Source-in-Cell Model for Gas-Droplet Flows," *J. Fluid Eng.*, 325 (1977).

Dasgupta, S., R. Jackson, and S. Sundaresan, "Turbulent Gas-Particle Flow in Vertical Risers," *AIChE J.*, **40**, 215 (1994).

Donsì, G., and L. Sesti Osseo, "Gas-Solid Flow Pattern in a CFB Operated at High Gas Velocity," *Circ. Fluid. Bed Technol.*, **IV**, 577 (1993).

Dry, R. J., et al., "The Effect of Gas Inlet Geometry on Gas-Solid Contact Efficiency in a CFB," *Proc. Eng. Found. Conf. Fluidization*, p. 211 (1992).

Grace. S. R., "High Velocity Fluidized Bed Reactors," *Chem. Eng. Sci.*, **45**, 1953 (1990).

Koyama, H., and J. S. Dranoff, "Modelling the Thermal Cracking of Ethane and Propane in a Non-Isothermal Vertical Pneumatic Transport Reactor," *Ind. Eng. Chem. Res.*, **31**, 2265 (1992).

Lam, C. K. G., and K. A. Bremhorst, "Modified Form of the K-ϵ Model for Predicting Wall Turbulence," *J. Fluid Eng.*, **103**, 456 (1981).

Louge, M., E. Mastorakos, and J. T. Jenkins, "The Role of Particle Collisions in Pneumatic Transport," *J. Fluid Mech.*, **231**, 345 (1991).

Patel, V. C., W. Rodi, and G. Scheurer, "Turbulence Models for Near Wall and Low-Reynolds Number Flows: A Review," *AIAA J.*, **23**, 1308 (1985).

Pita, J. A., and S. Sundaresan, "Gas-Solid Flow in Vertical Tubes," *AIChE J.*, **37**, 1009 (1991).

Pita, J. A., and S. Sundaresan, "Developing Flow of a Gas-Particle Mixture in a Vertical Riser," *AIChE J.*, **39**, 541 (1993).

Rizk, M. A., and S. E. Elghobashi, "A Two-Equation Turbulence Model for Dispersed Dilute Confined Two-Phase Flows," *Int. J. Multiphase Flow*, **15**, 119 (1989).

Rosten, H. I., and D. B. Spalding, *The Phoenics Reference Manual*, CHAM Tech. Rep. TR/200 (1987).

Sinclair, J. L., and R. Jackson, "Gas-Particle Flow in a Vertical Pipe with Particle-Particle Interactions," *AIChE J.*, **35**, 1473 (1989).

Tinaburri, A., M. Schenato, and A. Chicconi, "Experimental Results on a Pressurized CFB Plant Operated at High Velocity and Solid Flux," *Proc. Int. Conf. Multiphase Flow in Industrial Plants*, in press (1996).

Tu, J. Y., and C. A. J. Fletcher, "Numerical Computation of Turbulent Gas-Solid Particle Flow in a 90° Bend," *AIChE J.*, **41**, 2187 (1995).

Werther, J., "Fluid Mechanics of Large Scale CFB Units," *Cir. Fluid. Bed Technol.*, **IV**, 1 (1993).

Manuscript received July 10, 1995, and revision received June 7, 1996.